Recovirus NS1-2 has viroporin activity that induces aberrant cellular calcium signaling to facilitate virus replication

Alicia C. Strtak[1], Jacob L. Perry[1], Mark N. Sharp[1,4], Alexandra L. Chang-Graham[1], Tibor Farkas[2,3], and Joseph M. Hyser[1*]

[1]Alkek Center for Metagenomic and Microbiome Research and Department of Molecular Virology and Microbiology, Baylor College of Medicine, Houston, TX 77303. [2]Department of Pathobiological Sciences, Louisiana State University School of Veterinary Medicine, and [3]Louisinan Animal Disease Diagnostic Laboratory, Baton Rouge, LA 70803. [4]Texas Medical Center Summer Research Internship Program, Augustana College, Rock Island, IL 61201.

Correspondence should be sent to:
Joseph M. Hyser
Alkek Center for Metagenomic and Microbiome Research
Department of Molecular Virology and Microbiology
MS: BCM385
Baylor College of Medicine
Houston, TX, 77303
PH: 713-798-4514
FAX: 713-798-3586
Joseph.Hyser@bcm.edu

No conflicts of interest exist.

27   **Abstract**

28   Enteric viruses in the *Caliciviridae* family cause acute gastroenteritis in humans and animals, but

29   the cellular processes needed for virus replication and disease remain unknown. A common

30   strategy among enteric viruses, including rotaviruses and enteroviruses, is to encode a viral ion

31   channel (i.e., viroporin) that is targeted to the endoplasmic reticulum (ER) and disrupts host

32   calcium (Ca^{2+}) homeostasis. Previous reports have demonstrated genetic and functional

33   similarities between the nonstructural proteins of caliciviruses and enteroviruses, including the

34   calicivirus NS1-2 protein and the 2B viroporin of enteroviruses. However, it is unknown whether

35   caliciviruses alter Ca^{2+} homeostasis for virus replication or whether the NS1-2 protein has

36   viroporin activity like its enterovirus counterpart. To address these questions, we used Tulane

37   virus (TV), a rhesus enteric calicivirus, to examine Ca^{2+} signaling during infection and determine

38   whether NS1-2 has viroporin activity that disrupts Ca^{2+} homeostasis. We found that TV disrupts

39   increases Ca^{2+} signaling during infection and increased cytoplasmic Ca^{2+} levels is important for

40   efficient replication. Further, TV NS1-2 localizes to the endoplasmic reticulum (ER), the

41   predominant intracellular Ca^{2+} store and the NS2 region has characteristics of a viroporin domain

42   (VPD). NS1-2 had viroporin activity in a classic bacterial functional assay and caused aberrant

43   Ca^{2+} signaling when expressed in mammalian cells, but truncation of the VPD abrogated these

44   functions. Together, our data provide new mechanistic insights into the function of the NS2

45   region of NS1-2 and show that like many other enteric viruses, enteric caliciviruses also exploit

46   host Ca^{2+} signaling to facilitate their replication.

47   **Importance**

48   Tulane virus is one of many enteric caliciviruses that cause acute gastroenteritis and diarrheal

49   disease. Globally, enteric caliciviruses affect both humans and animals and result in >65 billion

50   dollars per year in treatment and healthcare-associated costs, thus imposing an enormous

51   economic burden. Recent progress has resulted in several cultivation systems (B cell, enteroid

52   and zebrafish larvae) to study human noroviruses, but mechanistic insights into the viral factors

53   and host pathways important for enteric calicivirus replication and infection are largely still

54   lacking. Here we used Tulane virus, a calicivirus that is biologically similar to human

55   noroviruses and can be cultivated in conventional cell culture, to identify and functionally

56   validate NS1-2 as an enteric calicivirus viroporin. Viroporin-mediated calcium signaling may be

57   a broadly utilized pathway for enteric virus replication, and its existence within caliciviruses

58   provides a novel approach to developing antivirals and comprehensive therapeutics for enteric

59   calicivirus diarrheal disease outbreaks.

60

Introduction

The *Caliciviridae* family consists of small, non-enveloped single-stranded RNA viruses with five major genera: *Sapovirus, Lagovirus, Vesivirus, Nebovirus,* and *Norovirus* (1, 2). Caliciviruses infect a wide-array of hosts and have importance in medical, veterinary, and agricultural fields (3). Of particular importance are human noroviruses (HuNoVs) that are the leading cause of acute gastroenteritis (AGE) in every age group, and can cause life-threatening illness in the young, immunocompromised, and elderly subpopulations (4–7). Estimates show that every individual will experience at least five symptomatic norovirus infections in their life (8), which underlines the need for anti-viral drugs, vaccines, or anti-diarrheal therapies for HuNoV infection (9, 10). However, many aspects of calicivirus pathogenesis, including that of HuNoV, remain uncharacterized, which represents a challenge to developing effective therapies (4, 6, 9). One strategy to address this challenge is to study other enteric caliciviruses, such as porcine sapoviruses and rhesus enteric caliciviruses (*Recovirus*). Recoviruses are a new proposed genus of enteric CVs initially identified in the stool from rhesus macaques, of which Tulane virus (TV) is the prototype strain (11, 12). While Recoviruses constitute a separate genus, these viruses are most closely related to HuNoVs and studies of TV show that it retains both biologic and genetic similarities to HuNoVs, including genomic organization, tissue tropism (intestinal epithelia), and clinical presentation (self-limiting vomiting and diarrhea) (1, 11–13). Furthermore, TV robustly replicates in cell culture in monkey kidney cell lines (e.g., LLC-MK2 cells), which facilitates investigation into the host pathways exploited by TV during infection. This makes TV an excellent model system to identify host signaling pathways broadly exploited by caliciviruses for replication and pathogenesis.

83   Like other caliciviruses, TV has 3 main open reading frames (ORFs), with ORF1

84   encoding the nonstructural proteins (NS1-7), and ORFs2-3 encoding the capsid proteins VPI

85   (ORF2) and VP2 (ORF3) (10, 14-15). During replication ORF1 is synthesized into the

86   polyprotein, which is subsequently cleaved by the viral protease NS6 to produce six

87   nonstructural proteins that orchestrate viral replication (4, 12, 14–16). In particular, the roles of

88   the NS1-2 protein (N-terminal protein) plays in viral replication and pathogenesis are not well-

89   characterized. Recent reports have identified that murine norovirus NS1, the N-terminal portion

90   of NS1-2, antagonizes the interferon pathway, but studies of full-length NS1-2 or the NS2

91   domain remain limited (17–19). Recombinant expression of NS1-2 from feline calicivirus

92   (FCV), murine norovirus (MNV), and HuNoV GII.4 shows that the protein traffics to the

93   endoplasmic reticulum (ER), concentrates perinuclearly, colocalizes with the ER-resident protein

94   calnexin, and contains C-terminal hydrophobic sequences (20–22). In contrast, Norwalk virus

95   (GI.1) NS1-2 (p48) was primarily found in the Golgi apparatus and implicated in disrupting ER-

96   to-Golgi trafficking (23, 24). The similarities in ER/Golgi membrane association and domain

97   organization of NS1-2 from different viruses suggest that NS1-2 may have a conserved function

98   among caliciviruses.

99   The ER, and to a lesser extent Golgi apparatus, are important intracellular calcium (Ca^{2+})

100   storage organelles, with the ER Ca^{2+} concentration being up to 1 mM (25, 26). As a ubiquitous

101   secondary messenger, Ca^{2+} is at the epicenter of many cellular processes and host machinery

102   tightly regulates Ca^{2+} levels to ensure low (nM) cytoplasmic Ca^{2+} concentrations at cellular rest

103   (26–32). Importantly, Ca^{2+} signaling regulates several aspects of viral life cycles including entry,

104   genome replication, and release (30, 33–35). To exploit Ca^{2+} signaling, many viruses express an

105   ion channel (i.e., viroporin) to dysregulate Ca^{2+} homeostasis in order to usurp Ca^{2+}-dependent

106   host processes (30, 36–39). The best characterized Ca^{2+} disrupting viroporins are the

107   nonstructural protein 4 (NSP4) from rotavirus (RV) and the 2B nonstructural protein of

108   enteroviruses (EV) and some other picornaviruses (36, 37, 40–44). Like all *bona fide* viroporins,

109   NSP4 and 2B have canonical biophysical motifs, including being oligomeric, having an

110   amphipathic α-helix that forms the pore, and a cluster of basic residues that facilitate membrane

111   insertion (37–39, 42–44). While no study has specifically looked at whether caliciviruses

112   dysregulate Ca^{2+} signaling or have a viroporin, they belong to the picornavirus-like superfamily

113   of positive-sense RNA viruses, among which there is considerable positional homology of the

114   cognate proteins of the nonstructural polyprotein (23, 45, 46). Within this rubric, the

115   picornavirus 2AB region constitutes the positional homolog of the calicivirus NS1-2 protein, and

116   several sequence motifs in the NS1 are conserved in the 2A protein of some picronaviruses (23).

117   While no functional homology between EV 2B and the NS2 region of NS1-2 has been yet been

118   identified, it is tempting to speculate that NS1-2 may have viroporin activity and dysregulate

119   host Ca^{2+} signaling analogous to that of EV 2B proteins.

120   In this study, we investigated the role of Ca^{2+} signaling in TV replication and whether TV

121   NS1-2 has viroporin activity that can dysregulate Ca^{2+} homeostasis. Using long-term live-cell

122   Ca^{2+} imaging, we sought to determine whether TV infection causes aberrant Ca^{2+} signaling

123   during infection and identify the cellular Ca^{2+} pools critical for the TV-induced Ca^{2+} signaling.

124   Finally, we tested TV NS1-2 for viroporin activity and determined whether the putative NS1-2

125   viroporin domain caused aberrant Ca^{2+} signaling similar to TV infection.

126

127   **Methods**

128   **Cell lines, GECI lentiviruses, and viruses:** All experiments were performed in LLC-MK2

129   cells. Lentivirus packaging and recombinant protein expression for western blot lysate

130   production was performed in HEK293FT cells (ATCC CRL-3216). Cell lines were grown in

131   high-glucose DMEM (Sigma: D6429) containing 10% fetal bovine serum (FBS) (Corning lot no.

132   35010167) and antibiotic/antimycotic (Invitrogen), and maintained at 37°C with 5% CO_2.

133   Lentivirus packaging in HEK293FT cells was performed as previously described (41). Briefly,

134   LLC-MK2 cells were transduced with a lentivirus vector encoding GCaMP6s 1-day post-seeding

135   (~85% confluency). We confirmed positive expression of GCaMP6s at 48-72 hours post-

136   transduction, then passaged cells 1:2 and added hygromycin (100 μg/mL) for selection of the

137   LLC-MK2-GCaMP6s cell lines, henceforth referred to as MK2- G6s. We determined GCaMP6s

138   activity and dynamic range using thapsigargin (0.5μM). Tulane virus (TV) stocks were made in-

139   house by infecting cells with MOI 0.01 and harvesting at ~95% cytopathic effect (CPE). Virus

140   titer was determined by plaque assay. Irradiated virus controls were made by gamma-irradiating

141   TV stocks for 19 hours.

142

143   **Replication assays:** LLC-MK2 cells were seeded at 125,000 cells/well in 24 well plates (Costar

144   3524, Corning) and inoculated next day with TV at MOI 1 for 1 hour. Inoculum was removed,

145   and cell media was replaced containing different extracellular Ca^{2+} conditions (0 mM Ca^{2+}, 4

146   mM Ca^{2+}), intracellular Ca^{2+} chelator 50 μM BAPTA-AM, or the sarco/endoplasmic reticulum

147   calcium ATPase (SERCA) blocker thapsigargin (TG). Ca^{2+}-free DMEM was purchased from

148   Gibco (Cat #21068-028). Standard high-glucose DMEM (Sigma) has 1.8 mM $CaCl_2$, which we

149   refer to as "2 mM Ca^{2+}, and media with 4 mM Ca^{2+} was made by adding 2 mM $CaCl_2$ to the

150   standard high-glucose DMEM (Sigma). We maintained TV-infected cells under these conditions

151   until the positive control (normal media) had ~90% CPE. Progeny virus was harvested by 3

152   freeze/thaw cycles, the virus yield was determined by plaque assay. For plaque assays, cells are

153   seeded at 75,000 cells/well in 24 well plates and 2-days post-seeding, the cells were inoculated

154   for 1 hour with 10-fold serial dilutions of the sample. Then, we removed the inoculum and added

155   the overlay. Overlays for plaque assays was made mixing equal parts 1.2% Avicel (FMC

156   Corporation) and 2X DMEM (Gibco). Plaque assays were harvested at 72 hours; fixed and

157   stained with crystal violet (3% solution) to visualize plaques. Titer is represented as plaque

158   forming units per milliliter (PFU/mL).

159

160   **One-step growth curves:** One step growth curves for TV were performed using a modified

161   protocol from previous reports (11, 15). Briefly, LLC-MK2 cells were inoculated with TV at

162   MOI 1 in serum-free DMEM (0% FBS DMEM). At 1-hour post-infection (HPI), the inoculum

163   was removed and replaced with 0% FBS DMEM. Cells were harvested at 0, 4, 6, 8, 10, 12, 16,

164   20, 24, and 28 HPI and virus yield determined by plaque assay. Each biological replicate was

165   performed in duplicate.

166

167   **Long-term Ca^{2+} imaging experiments:** Calcium imaging experiments were set up by adapting

168   a protocol detailed in previous reports (47). MK2-G6s cells were seeded at 78,500 cells/well in

169   15 μ-slide 8 well chambers (Ibidi, Germany) and infected the next day with TV at the indicated

170   MOI. After one hour, the inoculum was removed and replaced with FluoroBrite DMEM (Gibco).

171   For studies involving pharmacological compounds, the FluoroBrite was mixed with DMSO

172   (0.1%, vehicle control) or the indicated pharmacological compounds dissolved in DMSO. Then

173   the slide was mounted into a stage-top environmental chamber (Okolab H301-Mini) that

174   maintained 37°C with humidity control and 5% CO_2. Time lapse live-cell Ca^{2+} imaging

175   experiments were conducted for from ~2 HPI until ~18-24 HPI on a Nikon TiE epifluorescence

176   microscope using a SPECTRAX LED light source (Lumencor) and a 20X Plan Apo (NA 0.75)

177   objective. Images were acquired at 1-2 images/minute. Images were acquired and analyzed using

178   the NIS elements advanced research software package (Nikon). Prior to image analysis,

179   background camera noise was subtracted from the images using an averaged file of 10 no-light

180   camera images. Cells that underwent division during the imaging run were excluded from

181   analysis. Intracellular Ca^{2+} signaling over time was quantified by calculating the number of Ca^{2+}

182   spikes per cell. This was determined as follows: Raw fluorescence intensity values were

183   measured in Nikon software, then exported to Microsoft Excel to normalize the fluorescence to

184   the first image (F/F_0). The Ca^{2+} spikes were calculated by subtracting each normalized

185   fluorescence measurement from the previous measurement to determine the change in GCaMP6s

186   fluorescence (ΔF) between each timepoint. Ca^{2+} signals with a ΔF magnitude of >5% were

187   counted as Ca^{2+} spikes. For each condition testes, Ca^{2+} spikes in $\geq$30 cells were determined.

188

189   **Heatmap generation:** To generate heatmaps of the normalized GCaMP6s fluorescence over

190   time for long-term Ca^{2+} imaging experiments we used the TidyR (48) and ggplot2 (49) packages

191   available through R studio. Normalized GCaMP6s data from Excel was used to create a R-

192   compatible file (.csv) containing the normalized fluorescence and the acquisition time data for

193   the dataset, and imported the file into R. We used the TidyR package to organize data into a

194   format accessible by ggplot2. We then used ggplot2 to generate heatmaps.

195

196 **Prediction of viroporin motifs *in silico*:** We used the Hydropathy Analysis program at the

197 Transporter Classification Database to generate Kyte & Doolittle Hydropathy and Amphipathic

198 moment plots to identify putative viroporin motifs within full-length TV NS1-2 (50). Secondary

199 structure, membrane topology, and membrane integration predictions were performed using

200 PSIPred prediction analysis suite (website: http://bioinf.cs.ucl.ac.uk/introduction/) (51). Helical

201 wheel plots to identify clustered basic residues within the putative viroporin domain were

202 generated using the PepWheel analysis program at Heliquest (website:

203 http://heliquest.ipmc.cnrs.fr/) (52).

204

205 **Expression vectors:** *E. coli* expression constructs for the lysis assay were generated via ligation-

206 independent cloning (LIC) using the pET46-Ek/LIC kit (MilliporeSigma, Darmstadt, Germany).

207 The pET46-Ek/LIC constructs all have an N-terminal 6x histidine tag. Mammalian expression

208 vectors were generated by inserting c-myc tag and mRuby3 red fluorescent protein upstream of

209 full length NS1-2 and then subcloning this into the pTagRFP-N vector in place of TagRFP

210 (Epoch Life Sciences, Missouri City, TX). This construct will be referred to as RFP-NS1-2. The

211 NS1-2(Δ176) and NS1-2(Δ157) truncation mutations in both bacterial and mammalian

212 expression vectors were generated using the NEB Q5 site-directed mutagenesis kit (New

213 England Biolabs, Ipswich, MA). All constructs were sequence-verified using universal primers

214 specific to the construct backbone (GENEWIZ, South Plainfield, NJ). The mammalian

215 expression vector for EV 2B was generated by cloning the 2B from enterovirus 71 upstream into

216 pTagRFP-N and the construction of the NSP4-TagRFP expression vector was previously

217 described (53).

218

219 **Transfection experiments:** MK2-G6s cells were seeded in 15 μ-slide 8 well chambers (Ibidi,

220 Germany) and at 85% confluency transfected with mammalian expression constructs in Opti-

221 MEM (ThermoFisher) and Lipofectamine 2000 (Invitrogen). Transfection was optimized so cells

222 received 400 ng plasmid DNA and 0.5 μL of Lipofectamine 2000 per well. 10 μM trichostatin A

223 (TSA) was added from 1-3 hours post-transfection. TSA is a histone deacetylase (HDAC)

224 inhibitor used to increase expression from the vectors (54–56). Time-lapse Ca^{2+} imaging was

225 performed beginning 8 hours post-transfection to capture expression kinetics, and up to 24 hours

226 post-transfection to measure changes in Ca^{2+} signaling during expression of the RFP-tagged

227 proteins.

228

229 **Deconvolution microscopy:** LLC-MK2 cells were seeded in 15 μ-slide 8 well chambers (Ibidi,

230 Germany) and transfected one day prior to imaging. Cells were transfected with intracellular

231 markers for the plasma membrane (LCK-GFP; Addgene plasmid #61099), endoplasmic

232 reticulum (pLV-ER GFP; Addgene plasmid #80069), Golgi apparatus (pLV-Golgi GFP;

233 Addgene plasmid #79809), and mitochondria (HyPer-dMito, Envrogen). Control wells received

234 TagRFP (Envrogen), while experimental wells received either full length RFP-NS1-2, RFP-NS1-

235 2(Δ157) or RFP-NS1-2(Δ176). Cells were imaged 24 hours post-transfection on the DeltaVision

236 LIVE high resolution deconvolution microscope (GE Healthcare) using the 60X/1.4 Plan-Apo

237 NA oil objective (Olympus), and acquired using a pco.edge sCMOS_5.5 camera. Images were

238 acquired and deconvolved in SoftWoRx software. Upon deconvolving, images were further

239 processed in FIJI (ImageJ) to adjust for brightness/contrast and pseudo-coloring (57).

240

241   *E. coli* **Lysis Assay**: *E. coli* Lysis assays were performed as previously described (41). Briefly,

242   pET46-Ek/LIC constructs of the TV NS1-2 full-length and truncation mutants were transformed

243   into BL21(DE3)pLysS cells. Transformations were plated on LB + 1% glucose + 100μg/mL

244   ampicillin, + 35μg/mL chloramphenicol and grown at 37°C overnight. Isolated colonies were

245   picked next day and cultured overnight in liquid LB + 1% glucose, + 100μg/mL ampicillin, +

246   35μg/mL chloramphenicol at 37°C in an orbital shaker at 250 rpm. The next day, overnight

247   cultures were subcultured by 1:100 dilution into 200 mL LB + 1% glucose, + 100μg/mL

248   ampicillin, + 35μg/mL chloramphenicol. Subcultures were grown at 37°C in an orbital shaker at

249   250 rpm for ~3 hours to an OD_{630} between 0.3-0.5, then induced with 1mM IPTG. Absorbance

250   measurements at 630 nm (OD_{630}) were taken every 10 minutes for 90 minutes and normalized to

251   the induction OD_{630} to determine the percent growth or lysis over time after induction. Each

252   experiment was performed ≥3 times. Protein expression was determined by SDS-PAGE using a

253   4-20% Tris-glycine gel (Bio-RAD, Hercules, CA) and western blot for the 6x histidine tag. An

254   uninduced culture served as the negative control for viroporin activity and NS1-2 synthesis.

255

256   **Membrane association experiment:** Membrane association experiments were performed using

257   a modified protocol from previously reported experiments (36, 41). Lysed membranes from a

258   200 mL culture were centrifugated at 21,000 x g for 20 minutes and supernatants decanted.

259   Pellets were resuspended in PBS and sonicated 3 times for 1 minute on ice. Total lysate was

260   collected after sonication. Then membranes were pelleted by ultracentrifugation at 49,000 x g for

261   1 hour using a TLA-100.3 rotor in an Optima TL Ultracentrifuge (Beckman Coulter,

262   Indianapolis, IN), and the supernatant was collected for the soluble fraction. Finally, the

263   membrane fraction pellet was resuspended in PBS + 1% SDS to solubilize membrane proteins.

264   Samples from the total lysate, soluble fraction, and membrane fraction analyzed by western blot.

265

266   **Production of TV and Vpg antisera:** For the anti-TV antisera to detect VP1, adult male and

267   female CD-1 mice (purchased from Center for Comparative Medicine, Baylor College of

268   Medicine) were immunized 5 times with $CsCl_2$-gradient-purified TV at 10 μg/dose in AddaVax

269   adjuvant (InvivoGen). Immunizations were given at 3-week intervals. For the anti-Vpg antisera,

270   adult Balb/C were immunized 3 times with 10-20 μg/dose purified Vpg expressed in *E. coli*. The

271   priming dose was given in Freund's complete adjuvant and the subsequent boosts were given in

272   Freund's incomplete adjuvant. All experiments were performed in accordance with the

273   recommendations in the Guide for the Care and Use of Laboratory Animals of the National

274   Institutes of Health.

275

276   **Immunoblot analysis:** Samples were prepared using procedures adapted from (36). Briefly,

277   samples were mixed with 5X sample buffer containing 2-mercaptonethanol and boiled for 10

278   minutes at 100°C. Samples were then run on a 4-20% Tris-glycine gel (Bio-RAD, Hercules CA)

279   and transferred onto a nitrocellulose membrane using the Transblot Turbo transfer system (BIO-

280   RAD, Hercules, CA). To detect the bacterial constructs of NS1-2 and NSP4, we used the mouse

281   α-HIS Tag monoclonal antibody at 1:1000 (Genscript, Piscataway, NJ). To detect mammalian

282   expression constructs of NS1-2, we used the mouse α-c-Myc monoclonal (clone 9E10) antibody

283   at 1:1000 (R&D Systems, MN). To detect TV structural protein VP1, we used the mouse α-TV

284   polyclonal we made in-house by hyperimmunizing CD1 mice with purified TV particles. To

285   detect TV nonstructural protein Vpg, we used the mouse α-Vpg polyclonal antibody made by

286   hyperimmunizing mice with bacterially expressed and purified Vpg. For loading control of

287   mammalian cell lysates, we used the mouse α-GAPDH at 1:3000 (Novus Biologicals, CO). We

288   used alkaline phosphatase-conjugated goat α-mouse IgG at 1:2000 (Southern Biotech,

289   Birmingham, AL), and visualized using alkaline phosphatase substrate [Tris-base, nitro blue

290   tetrazolium (NBT), 5-bromo-4-chloro-3-indolyl phosphate (BCIP)].

291

292   **Statistical analysis:** Statistical analyses were completed using GraphPad Prism (ver. 7.03). Data

293   in this manuscript is presented as mean ± standard deviation. We performed columns statistics to

294   collect descriptive statistics and to determine the normality of the datasets. We then used the

295   unpaired Student's t-test for datasets with a parametric distribution, or a Mann-Whitney test for

296   datasets with a nonparametric distribution. Differences were determined statistically significant

297   if the $p < 0.05$. Authors had access to the data for this manuscript, and all authors approved the

298   final manuscript.

299   **Data availability:** RConsole code for the heatmaps generated in this paper is available upon

300   request.

301 **Results**

302 **TV infection disrupts host calcium signaling kinetics in LLC-MK2 cells.** Ca^{2+} is a ubiquitous

303 secondary messenger and many enteric viruses (*e.g.*, RVs and EVs) require elevated cytosolic

304 Ca^{2+} to facilitate replication (30, 36–39, 42, 43). To determine if TV causes aberrant Ca^{2+}

305 signaling like other enteric viruses, we examined whether Ca^{2+} signaling dynamics changed

306 during TV infection. We infected LLC-MK2 cells stably expressing GCaMP6s (MK2-G6s) with

307 different infectious doses [multiplicity of infection (MOI) 1, 5, 10] or γ-irradiated inactivated TV

308 and performed live-cell fluorescent microscopy during the infection. GCaMP6s is a GFP-based

309 genetically encoded Ca^{2+} indicator that reports changes in cytosolic Ca^{2+} as an increase in

310 fluorescence (58). TV-infected MK2-G6s cells show increased cytoplasmic Ca^{2+} levels (Fig. 1A)

311 beginning at roughly 8 HPI (MOI 10) and progressing for the remainder of the infection

312 (Supplemental Video S1). The observed increase in Ca^{2+} signaling coincides with the synthesis

313 of TV nonstructural proteins, assessed by western blot using an α-Vpg antisera (Fig. 1B) and TV

314 structural proteins, assessed by western blot using an α-TV antisera to detect VP1 (Fig. 1C),

315 which show increased TV protein production between 8-12 HPI. Further, based on a one-step

316 growth curve, the increased cytosolic Ca^{2+} also coincides with the onset of progeny virus

317 production, which occurs between 6-8 HPI (Fig. 1D). The increases in cytosolic Ca^{2+} were

318 dynamic during TV infection (Supplemental Video S2). In infected cells, we noted that changes

319 in cytosolic Ca^{2+} occurred through an increased number of discrete Ca^{2+} signals, much like what

320 we recently observed in RV-infected cells (Fig. 1E) (47). We refer to these high-amplitude,

321 transient Ca^{2+} signals as "Ca^{2+} spikes" and quantitated the number of Ca^{2+} spikes per cell during

322 infection. Compared to uninfected controls, TV-infected cells have significantly more Ca^{2+}

323 spikes/cell, but cells inoculated with γ-irradiated TV did not exhibit increased Ca^{2+} signaling

324   (Fig. 1F). Together, these data indicate that increased Ca^{2+} signaling requires replication

325   competent virus and occurs at later during infection, well after entry has occurred. Additionally,

326   Ca^{2+} signaling in infected cells increases in an infectious dose-dependent manner, saturating at

327   MOI=5 (Fig. 1F). To visualize the aberrant Ca^{2+} signaling induced by TV, we generated

328   heatmaps plotting normalized GCaMP6s fluorescence over time (Fig. 1G). Heatmap data shows

329   an increased number and magnitude of Ca^{2+} signals and that cytosolic Ca^{2+} levels change earlier

330   and more frequently throughout infection as infectious dose increases (Fig. 1G). The heatmaps

331   also show that MK2-G6s cells inoculated with γ-irradiated TV do not have increased Ca^{2+}

332   signaling compared to mock-inoculated cells (Fig. 1G), consistent with the lack of increased

333   Ca^{2+} spikes (Fig. 1F). Taken together, these data suggest that, like other enteric viruses, TV

334   disrupts host Ca^{2+} signaling kinetics during infection.

335

336   **Intracellular Ca^{2+} is critical for TV replication.** Since we observed aberrant Ca^{2+} signaling

337   during TV infection, we sought to determine whether Ca^{2+} was involved in TV replication. To

338   test this, we manipulated extracellular and intracellular Ca^{2+} levels and determined their effect

339   this had on TV yield. Doubling the extracellular Ca^{2+} concentration (~4 mM) did not affect TV

340   yield (Fig. 2A, right). In contrast, TV propagated in Ca^{2+}-free media significantly reduced total

341   yield (Fig. 2A, middle). Interestingly, plaques of TV propagated in Ca^{2+}-free media were

342   substantially smaller than that propagated in normal media, even though the plaque assay

343   titrations were performed in normal media (Fig. 2C). Next, to investigate the role of intracellular

344   Ca^{2+} during infection, we treated LLC-MK2 cells with BAPTA-AM, which chelates cytosolic

345   Ca^{2+} and therefore buffers cytosolic Ca^{2+} (59, 60). TV replication in Ca^{2+}-free media

346   supplemented with BAPTA-AM ($0Ca^{2+}$/BAPTA) was reduced up to 4-log (Fig. 2B), which was

347   a greater inhibition than Ca^{2+}-free media alone (Fig. 2A versus 2B). We next sought to determine

348   whether intracellular Ca^{2+} stores are important for TV replication by testing the effect of

349   thapsigargin (TG) on TV replication. TG is an inhibitor of sarco/endoplasmic reticulum Ca^{2+}

350   ATPase (SERCA), which pumps cytosolic Ca^{2+} into the ER to help maintain ER Ca^{2+} stores. We

351   treated TV-infected cells with TG and measured TV yield as above and found that TV

352   replication is ~3-log less in TG-treated than in DMSO-treated cells (Fig. 2B). Finally, we tested

353   these different manipulations of extracellular or intracellular Ca^{2+} on TV yield a different time

354   points during infection (8, 16, 24 HPI) (Fig. 2D). These studies confirmed that reduction of

355   extracellular Ca^{2+} or treatment with TG significantly inhibited total virus replication; however,

356   the rate of progeny virus production was not substantially reduced. Together, the replication

357   assays demonstrate that intracellular Ca^{2+} levels facilitate TV replication, and that the ER Ca^{2+}

358   store is particularly important for robust virus production.

359

360   **TV-induced Ca^{2+} signaling requires ER Ca^{2+} stores.** We next sought to determine the effect

361   that the manipulations to extracellular and intracellular Ca^{2+} had on the TV-induced Ca^{2+}

362   signaling exhibited in Figure 1. We altered extracellular and intracellular Ca^{2+} concentrations as

363   above and performed live Ca^{2+} imaging of mock and TV-infected MK2-G6s cells. TV-infected

364   cells in 2 mM Ca^{2+} (normal media) exhibited increased Ca^{2+} signaling, as observed above (Fig.

365   3A). Supplementing media with additional extracellular Ca^{2+} (4 mM Ca^{2+} total) did not further

366   increase the Ca^{2+} spikes but removing extracellular Ca^{2+} abolished the TV-induced Ca^{2+} spikes

367   (Fig. 3A). Using heatmaps, we plotted the relative change in GCaMP6s fluorescence over time

368   and observed increased signaling starting at ~8 HPI in both the 2 mM Ca^{2+} and 4 mM Ca^{2+}

369   conditions (Fig. 3B). Further, the heatmaps show that infected cells in Ca^{2+}-free media have a

370   signaling profile that phenotypically mimics uninfected controls (Fig. 3B). Like the results

371   obtained in replication assays, buffering cytoplasmic Ca^{2+} using BAPTA-AM reduced the

372   number of Ca^{2+} spikes per cell to a level comparable to that of mock-infected cells (Fig. 3C)

373   (Supplemental Video S2). Similarly, blocking the ER SERCA pump with TG significantly

374   reduces TV-induced Ca^{2+} signaling (Fig. 3D), supporting replication data and demonstrating that

375   ER Ca^{2+} stores are a critical source of Ca^{2+} for enhancing replication.

376

377   **Tulane virus NS1-2 is targeted to the ER membrane**. Our data indicates that TV activates

378   aberrant Ca^{2+} signaling involving the ER Ca^{2+} store, much like the dysregulation of Ca^{2+}

379   homeostasis by other enteric viruses observed in RV and EV infections. Both RV and EV encode

380   a viroporin, or viral ion channel, that targets the ER Ca^{2+} store to activate aberrant Ca^{2+} signaling

381   pathways that are critical for virus replication (35, 36, 38, 39, 42, 43). Viroporins are integral

382   membrane proteins that have some common characteristics, including being oligomeric, having

383   an amphipathic α-helix that serves as the channel lumen through the membrane, and a cluster of

384   basic amino acid residues that facilitate insertion into the membrane (24, 34, 35, 39, 61).

385   Previous work with NS1-2 from several different caliciviruses shows it is membrane-associated

386   and primarily to the ER (17–20, 24) and/or Golgi (17, 20, 21, 23). Thus, we hypothesized that

387   calicivirus NS1-2 could be a viroporin involved in the aberrant Ca^{2+} signaling we observed

388   during TV infection. Notably, the calicivirus NS2 domain is the positional homolog of the EV

389   2B viroporin (Fig. S1). This is potentially significant because previous studies have found

390   conserved functional characteristics between the positional homologs of the other nonstructural

391   proteins (20, 21, 23, 46, 61–64), and functional homology between EV 2AB and human

392   norovirus (HuNoV) GII.4 NS1-2 (20, 23). Additionally, when performing multiple sequence

393   alignments of other calicivirus NS1-2s, we found that the C-terminal domain (CTD) of this

394   protein is highly conserved (Fig. S2). To determine whether TV NS1-2 has viroporin-like

395   characteristics, we examined TV NS1-2 for viroporin motifs. First, we performed a Kyte-

396   Doolittle plot to detect hydrophobic regions of NS1-2 and an amphipathicity plot to identify

397   potential amphipathic domains (Fig. 4A). We found that aa195-215 (Fig. 4A, dark green box) in

398   the CTD of NS1-2 has a high amphipathic moment. We then used PSIPred (51) to model NS1-2

399   predicted secondary structure (Fig. 4B). Output from this analysis suggested that the NS1-2 CTD

400   was predominantly comprised of alpha-helices (Fig. 4B, pink residues), and accompanying

401   confidence scores for prediction of these C-terminal helices were $\geq$75% (Fig. S3). Interestingly,

402   the region of peak amphipathicity (Fig. 4A) was located within one of the PSIPred helix

403   predictions of the CTD (Fig. 4B, dark green bar) and contained clustered basic residues (blue

404   asterisks), two key features of viroporins. Additionally, NS1-2 topology modeling identified two

405   putative transmembrane domains (TMD): the first (TMD1) from aa164-179, and the second

406   (TMD2) from aa202-225 (Fig. 4C, top). The membrane topology schematic indicated that both

407   TMD1 and TMD2 had predicted pore-lining regions within their helices (Fig. 4B bottom left).

408   To explore this, we used HeliQuest (52) to generate a helical wheel diagram for TMD2 (aa198-

409   215), since TMD2 had the clustered basic residues common among viroporins. The helical wheel

410   shows that TMD2 is highly amphipathic with clear polar and non-polar faces to the helix (Fig.

411   4D). The calculated hydrophobic moment for TMD2 is 0.522, supporting the above

412   amphipathicity predictions (Fig. 4A). Given the results of these computational studies, we

413   predicted that NS1-2 TMD2 (aa195-215) is a viroporin domain and set out to test this prediction

414   experimentally.

415   First, we tested whether TV NS1-2 was an integral membrane protein and whether it

416   localized to the ER similar to NS1-2 from other caliciviruses. To do so, we generated bacterial

417   and mammalian expression vectors of full-length NS1-2. For mammalian expression vectors, we

418   N-terminally fused full-length NS1-2 to mRuby3 (henceforth referred to as RFP-NS1-2). From

419   these constructs, we generated two truncation mutants of WT NS1-2 in both mammalian and

420   bacterial expression vectors: the first, NS1-2 Δ176, was predicted to have TMD1 but lack the

421   viroporin domain, and the second, NS1-2 Δ157, was predicted to lack both TMD1 and the VPD.

422   We then transfected wild-type, full-length (WT) RFP-NS1-2, RFP-NS1-2 Δ157, and RFP-NS1-2

423   Δ176 into HEK 293FT cells and harvested cell suspensions next day. Samples following cell

424   lysis, sonication, and fractionation were collected for SDS/PAGE western blots. We found both

425   Δ176 and WT TV NS1-2 in the total fraction (T) and membrane pellets (M), but not in the

426   supernatant (S), suggesting that TMD1 mediates membrane association (Fig. 4E). Additionally,

427   in the non-reducing, unboiled conditions used, oligomers of both both Δ176 and WT RFP-NS1-2

428   were detected by western blot (Fig 4E, arrowheads). Similar results were obtained from

429   membrane fractionation of analogous bacterially expressed NS1-2 constructs (Fig. S4). Using the

430   mammalian expression vectors of RFP-NS1-2, we performed colocalization assays with

431   fluorescent markers of the ER, Golgi apparatus, and mitochondria. RFP-NS1-2 showed no

432   colocalization with the Golgi or mitochondria (Fig. 4F). In contrast, RFP-NS1-2 strongly

433   colocalized with the ER-GFP marker (Fig. 4F), indicating that, like NS1-2 from other

434   caliciviruses and EV 2B and RV NSP4, TV NS1-2 traffics to the ER membrane.

435

436   **TV NS1-2 has viroporin activity that disrupts Ca^{2+} signaling.** Since our predictive modeling

437   suggested that NS1-2 met the biophysical requirements for a viroporin, and our live-cell Ca^{2+}

438   imaging data exhibited large changes in cytosolic Ca^{2+} during TV infection, we tested whether

439   NS1-2 has viroporin activity. We performed the *E. coli* lysis assay, which is a classical viroporin

440   functional assay, wherein viroporin expression by BL21(DE3)pLysS *E. coli* results in

441   permeabilization of the inner membrane, resulting in T7 lysozyme-mediated cell lysis (41). This

442   assay has been used to identify and initially characterize many viroporins (36, 65, 66). We

443   expressed full-length HisNS1-2 in BL21(DE3)pLysS cells and measured optical density (OD)

444   over time following protein induction with IPTG. For the lysis assay, strong viroporin activity is

445   characterized by large decreases in OD over time, whereas no viroporin activity is characterized

446   by increases in OD over time. Our results show that induced NS1-2 has strong viroporin activity,

447   similar to that of RV NSP4, our positive control for viroporin activity (Fig. 5A). We see no

448   changes in OD over time for uninduced NS1-2, indicating that HisNS1-2 viroporin activity

449   correlated with protein expression, detected by immunoblot for the 6xHis-tag (Fig. 5B). We then

450   asked whether recombinant expression of RFP-NS1-2 alone increases Ca^{2+} signaling in MK2-

451   G6s cells. To test this, we transfected MK2-G6s cells with mammalian expression vectors for

452   RFP-NS1-2 as well as RFP-NSP4 and RFP-EV 2B, our positive controls for viroporin-mediated

453   Ca^{2+} signaling. Expressing RFP-tagged viroporins in MK2-G6s cells significantly increases both

454   the number and amplitude of Ca^{2+} spikes. However, this was not observed in cells expressing

455   RFP alone, as illustrated by the representative single-cell traces (Fig. 5C) (Supplemental Video

456   S3). As above, we quantitated the number of Ca^{2+} spikes and confirmed that recombinant

457   expression of RFP-NS1-2 increased the number of Ca^{2+} spikes per cell approximately 2-fold,

458   similar to that of EV 2B and RV NSP4 (Fig. 5D). Taken together, our results demonstrate that

459   TV NS1-2 has viroporin activity in the lysis assay, similar to *bona fide* viroporins, and causes

460   aberrant host Ca^{2+} signaling when expressed in mammalian cells.

461

462 **NS1-2 viroporin activity maps to the putative viroporin domain**. Our computational studies

463 above identified a putative TV NS1-2 VPD from aa195-212. To determine whether the NS1-2

464 viroporin activity maps to this putative VPD, we generated C-terminal truncation mutants in

465 bacterial expression vectors with deletions after aa212 (A212-Δ), after aa194 (W194-Δ), or after

466 aa176 (D176-Δ) and characterized them in the lysis assay (Fig. 6A). We found that the A212-Δ

467 truncation (red) had strong lysis activity comparable to full-length NS1-2 (black) (Fig. 6B). In

468 contrast the D176-Δ truncation (blue) exhibited no lysis activity, comparable to uninduced NS1-

469 2 (grey) (Fig. 6B). Immunoblot analysis confirm that protein expression correlated with

470 viroporin activity, and that the impaired activity of W194-Δ was not due to lower expression

471 levels, since the expression was comparable to that of full-length and A212-Δ (Fig 6C). Since the

472 W194-Δ truncation (green) had impaired viroporin activity, this suggests that the VPD

473 functionally extends to aa177-212.

474 Next, we characterized truncation mutants for their activation of aberrant Ca^{2+} signaling

475 in MK2-G6s cells. Since recombinant expression of full-length RFP-NS1-2 induced aberrant

476 Ca^{2+} signaling (Fig. 5D), we tested whether truncating the putative viroporin domain alone

477 (Δ176) or both TMDs (Δ157) would compromise NS1-2-induced Ca^{2+} signaling (Fig. 6D). First,

478 we examined the subcellular distribution and expression levels of the constructs. While the full-

479 length and Δ176 truncation both appeared reticular, the Δ157 truncation had cytoplasmic

480 distribution, consistent with it lacking both TMDs (Fig. 6E). Immunoblot analysis shows that the

481 expression of both truncations was much greater than that of full-length NS1-2 (Fig. 6F, left

482 blots) and by loading less lysate we can better resolve the 2 kDa size difference in the Δ157 and

483 Δ176 truncations (Fig. 6F, right blots). Next, we examined whether these truncations could

484   induce Ca^{2+} signaling by long-term live Ca^{2+} imaging in MK2-G6s cells. Individual cell traces

485   illustrate that neither the $\Delta157$ nor the $\Delta176$ truncation dramatically increased Ca^{2+} signaling

486   similar to full-length RFP-NS1-2 (Fig. 6G). Quantitation of the Ca^{2+} spikes per cell showed that

487   while both truncations exhibited higher Ca^{2+} signaling than RFP alone (Fig 6G), the amplitude of

488   these spikes was significantly reduced compared to full-length RFP-NS1-2 (Fig. 6H). The

489   significant reduction in the number and amplitude of Ca^{2+} spikes/cell for both mutants highlights

490   the critical importance of an intact VPD for disrupting host Ca^{2+} signaling. Together this work

491   demonstrates that TV NS1-2 is an ER-targeted viroporin that induces aberrant Ca^{2+} signaling.

492

493 **Discussion**

494   As obligate intracellular pathogens, viruses are adept at exploiting host pathways to

495 facilitate replication. Viruses from many different taxonomic families activate aberrant Ca^{2+}

496 signaling because Ca^{2+} signals are used by all cells to regulate a vast array of cellular functions.

497 Therefore, this represents a powerful strategy to reconfigure host cell physiology via targeted

498 disruption of host Ca^{2+} homeostasis. The overarching goal of this study was to determine

499 whether dysregulation of Ca^{2+} signaling is a characteristic of caliciviruses and if this is due to the

500 production of a viroporin protein similar to picornaviruses. To address these questions, we

501 studied TV, as a model calicivirus, using a combination of live-cell Ca^{2+} imaging and other

502 classical techniques. The major new findings of this study are as follows: (i) TV infection causes

503 aberrant Ca^{2+} signaling that coincides with viral protein synthesis and replication, (ii) cellular

504 Ca^{2+} is critical for TV replication and buffering of cytosolic Ca^{2+} severely reduced viral yield,

505 (iii) TV NS1-2 has viroporin activity and dysregulates Ca^{2+} signaling in mammalian cells similar

506 to TV infection, and (iv) NS1-2 viroporin activity maps to a C-terminal integral membrane

507 viroporin domain and truncation of this domain abrogates the NS1-2-induced activation of Ca^{2+}

508 signaling. To our knowledge, these results are the first to show exploitation of Ca^{2+} signaling by

509 a calicivirus and identification of NS1-2 as a Ca^{2+}-disrupting viroporin. These findings further

510 extend the functional homology between the calicivirus nonstructural proteins and their

511 picornavirus positional homologs.

512   The exploitation of host Ca^{2+} signaling to facilitate virus replication is a common feature

513 of many viruses (30). Our finding that TV coopts Ca^{2+} signaling is consistent with previous

514 studies showing that elevated Ca^{2+} levels are important for picornavirus replication, especially

515 since caliciviruses and picornaviruses utilize a similar replication strategy (43). Similar to other

516   Ca^{2+}-disrupting viruses, TV also induces aberrant Ca^{2+} signaling peak of virus replication, many

517   hours after cell entry. This is consistent with the reduced virus yield in media with reduced

518   extracellular Ca^{2+} or treatments to buffer cytosolic Ca^{2+} (BAPTA-AM) or block refilling of ER

519   Ca^{2+} stores (TG). Further, as we recently reported for RV infection, the TV-induced increase in

520   cytosolic Ca^{2+} manifests as many discrete Ca^{2+} signals rather than a monophasic increase in Ca^{2+}

521   over the infection (47). This raises the question of what cellular pathways are activated by this

522   Ca^{2+} signaling and how they benefit TV replication. Both RV and EV have been shown to

523   exploit Ca^{2+} signaling to activate the biosynthetic early stages of autophagy, which facilitates

524   virus replication through rearrangement of cellular membranes to form replication complexes

525   (67). MNV infection of primary macrophages or RAW264.7 cell line activates autophagy, but, in

526   contrast to RV and EV, autophagy limits MNV replication (68). Thus, it remains to be

527   determined whether autophagy plays a role in calicivirus replication complex assembly or

528   whether Ca^{2+} signaling regulates autophagy activation during calicivirus infection. Further,

529   elevated Ca^{2+} signaling may serve to modulate cellular apoptotic responses. Strong monophasic

530   increases in cytosolic Ca^{2+} activate apoptosis through mitochondrial Ca^{2+} overload, but transient

531   and oscillatory Ca^{2+} fluxes serve as pro-survival signals (69). Activation of apoptosis has been

532   seen in norovirus and feline calicivirus-infected cells, and caspase activation is critical for

533   cleavage and release of MNV NS1 from NS1-2, which in turn modulates cellular innate immune

534   responses (19, 22). Thus, increased transient Ca^{2+} signaling may serve to counteract apoptosis

535   activation and help prolong cell viability to maximize virus replication.

536   Within the superfamily of picornavirus-like positive sense RNA viruses, there is

537   positional homology between the ORF1 nonstructural proteins of caliciviruses (and likely

538   astroviruses) and the P2-P3 nonstructural proteins of picronaviruses (23, 45, 46). We used this

539   framework to determine whether TV NS1-2 exhibited viroporin activity, since the positional

540   homolog, the picornavirus 2B protein, is a well-established Ca^{2+}-conducting viroporin (34, 44).

541   We found that TV NS1-2 has viroporin activity, similar to 2B and RV NSP4, and the viroporin

542   activity mapped to the integral membrane NS2 domains. Since both the N- and C-termini are

543   likely oriented in the cytoplasm, NS1-2 is classified as a Class II2 viroporin, similar to the

544   picornavirus 2B proteins (34, 44). This topology is supported by the cytosolic accessibility of the

545   NS1 domain and the need for the C-terminus to also be localized in the cytosol to enable

546   cleavage by the NS6 protease. This raises the question of whether NS1-2 viroporin activity is

547   conserved throughout the *Caliciviridae* family. Though 2B and NS1-2 lack appreciable primary

548   sequence homology, this is not surprising because viroporins, even from the same virus family,

549   often only share the common viroporin motifs (*i.e.*, having [i] an amphipathic α-helix, [ii] a

550   cluster of basic residues, and [iii] being oligomeric) (33, 38, 39). Among NS1-2 from different

551   caliciviruses, we found that these characteristic features are conserved, so we predict viroporin

552   activity of NS1-2 is a common function. Furthermore, since blunting cytosolic Ca^{2+} signaling

553   with BAPTA-AM reduced TV replication, blocking NS1-2 viroporin activity with mutations or

554   drugs should also reduce replication. This is supported by a previous study showing that

555   recombinant coxsackie B3 virus with mutations of the 2B viroporin exhibited significantly

556   impaired replication or were completely replication deficient (70). Analogous studies can be

557   done using the TV reverse genetics system once residues critical for viroporin activity can be

558   identified through mutagenesis screens of the TV NS1-2 viroporin domain we mapped in this

559   study.

560   The increased Ca^{2+} signaling observed in TV-infected cells is phenotypically similar to

561   that induced by recombinant expression of full-length NS1-2, but the Ca^{2+} signaling is abrogated

562   by truncation of the viroporin domain. Further, NS1-2 primarily localized to the ER, which is a

563   major intracellular Ca^{2+} storage organelle. Thus, our model predicts that NS1-2 directly releases

564   Ca^{2+} from the ER; however, it is likely that both NS1-2 and activation of host Ca^{2+} signaling

565   pathways contribute to the observed Ca^{2+} signals. Ca^{2+} signals from NS1-2 require it to directly

566   conduct Ca^{2+} and have a high enough conductance that the ER Ca^{2+} release event can be detected

567   by a fluorescent Ca^{2+} indicator, yet these unitary events are challenging to detect even for large

568   channels like the IP3R (71). Future studies using patch clamp electrophysiology are needed to

569   confirm that NS1-2 conducts Ca^{2+} and determine its conductivity. Nevertheless, based on the

570   similarities between NS1-2 and other Ca^{2+}-conducting viroporins, EV 2B and RV NSP4, NS1-2

571   viroporin activity would reduce ER Ca^{2+} levels and this in turn will activate host Ca^{2+} signaling

572   pathways. First, the moderately increased steady-state cytosolic Ca^{2+} levels could foster more ER

573   Ca^{2+} release by potentiating the IP3R Ca^{2+} release channel (72). Second, reduced ER Ca^{2+} levels

574   activate the store-operated Ca^{2+} entry (SOCE) pathway, wherein decreased ER Ca^{2+} levels

575   activate the ER Ca^{2+} sensing protein stromal interaction molecule 1 (STIM1). Activated STIM1

576   translocates to ER microdomains adjacent to the plasma membrane and opens Ca^{2+} influx

577   channels, like Orai1, to elevate cytosolic Ca^{2+} (31, 32). This Ca^{2+} influx, in concert with SERCA,

578   helps to refill ER stores for continued signaling.

579   HuNoV and human sapoviruses cause outbreaks of AGE and are a major cause of

580   foodborne illnesses. However, the molecular mechanisms of how these caliciviruses cause

581   vomiting and diarrhea, the chief symptoms of AGE, have not been characterized. The

582   dysregulation of Ca^{2+} signaling by TV may provide insights into the pathophysiology of enteric

583   caliciviruses. Both IP3-mediated ER Ca^{2+} release and SOCE have been shown to activate

584   chloride secretion from epithelial cells (73, 74). Additionally, in studies of other viroporins, the

585 viroporin-induced elevated cytosolic Ca^{2+} induces cytoskeleton rearrangement, leading to

586 disassembly of tight junctions and loss of barrier integrity (39). Hyperactivation of chloride

587 secretion and loss of tight junctions would contribute to excess fluid secretion and diarrhea. In

588 our study we have shown that dysregulated Ca^{2+} signaling is a feature of calicivirus infection

589 using TV. Thus, future studies can further examine the role of aberrant Ca^{2+} signaling in

590 calicivirus pathophysiology using human intestinal enteroid cultures that support the replication

591 of many HuNoV strains (4).

592   In summary, we have shown that TV activates aberrant Ca^{2+} singling during infection,

593 and cellular Ca^{2+} is critical for robust TV replication. Further, we found that the NS2 domain of

594 the NS1-2 nonstructural protein is a viroporin that alone induces Ca^{2+} signaling similar to TV

595 infection. Together, these results indicate that NS1-2 is functionally analogous to EV 2B and RV

596 NSP4. While little is known about the function(s) of NS1-2, and particularly the NS2 domain of

597 NS1-2, the similarity with other Ca^{2+} conducting viroporins may provide a broader insight for

598 understanding NS1-2 functions. Finally, antiviral drugs against viroporins have been developed

599 for influenza M2 and HIV Vpu (34). Thus, the NS1-2 viroporin may be a viable antiviral drug

600 target against caliciviruses.

601

611

612 **Primers:**

Primer name	Sequence
pET-46 EK/LIC NS1-2 Fwd	GACGACGACAAGATGGATACGTCCATAGATTCTGTGTTATCTGACACCAGC
pET-46 EK/LIC NS1-2 Rev	GAGGAGAAGCCCGGTTACTGTGGGATCAGTGATGAGGTAAGAAATGTGATCAAACTGG
pET-46 EK/LIC NS1-2 D176 Rev	GACGACAAGCCCGGTTAATCTTTGACAATAAGGTACACGATCTCGAG
pET-46 EK/LIC NS1-2 W194 Rev	GAGGAGAAGCCCGGTTACCAATTGTGCCAAAGGTTC
pET-46 EK/LIC NS1-2 A212 Rev	GAGGAGAAGCCCGGTTAAGCAACCCTTGTCAGGAATG
pET-46 EK/LIC NS1-2 Truncations Fwd	GACGACGACAAGATGGATACGTCCATAGATTCTGTGTTATC
pET-46 EK/LIC NS1-2 Δ157 Rev	GAGGAGAAGCCCGGTTTATTTGGTCCCTCCGACG
pET-46 EK/LIC NS1-2 Δ176 Rev	GAGGAGAAGCCCGGTTTAATTGACATCTTTGACAATGAGG
pTagRFP-N mRuby3-NS1-2 Δ157 Q5 Mut. Fwd	CGGAGGGACCTAAAGCGGATGGAC
pTagRFP-N mRuby3-NS1-2 Δ157 Q5 Mut. Rev	GTCGTACCTATTTTCATTCCAATCTTGGACATGTGTG
pTagRFP-N mRuby3-NS1-2 Δ176 Q5 Mut. Fwd	CAAAGATGTCTAATGGGCAAAGATTTG
pTagRFP-N mRuby3-NS1-2 Δ176 Q5 Mut. Rev	ACAATGAGGTACACGATCTCGAG

613

614
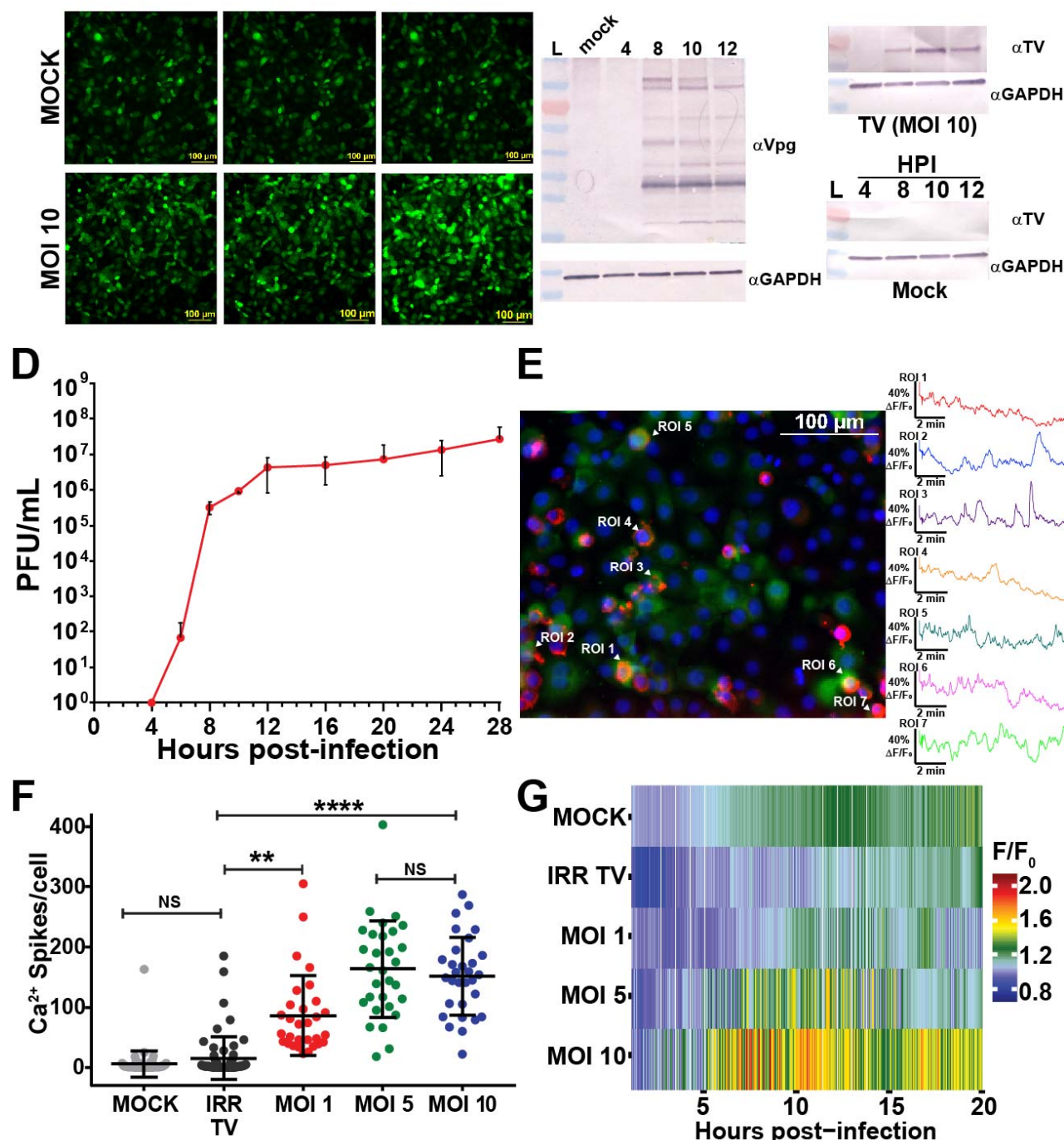
Figure 1 TV infection disrupts host calcium signaling kinetics in LLC-MK2 cells.
A. Representative images at early (4 HPI), onset (8 HPI), and late (12 HPI) stages of mock (top) and TV-infected (bottom) LLC-MK2 GCaMP6s cells. **B, C.** Western blots for nonstructural protein Vpg (B) and structural protein VP1 (C) confirm that aberrant Ca^{2+} signaling in infected cells coincides with both structural and nonstructural protein synthesis. **D**. One-step growth curve for TV at a low MOI (1) shows that virus replication is concomitant with viral protein synthesis (1B, C) and with changes in Ca^{2+} signaling (1A). **E.** Still from overlay of α-Vpg staining (red) onto

623   short (10 minute) continuous imaging runs of TV-infected cells (MOI=5) 12 HPI. Accompanying
624   Ca^{2+} cell traces (right) shows the dynamic increases in cytosolic Ca^{2+} in infected cells **F.** Compared
625   to mock, TV-infected cells have an increased number of Ca^{2+} spikes per cell that increases in an
626   infectious dose-dependent manner, saturating at MOI=5. **G.** Heatmap data suggests that Ca^{2+}
627   signaling increases with infectious dose, and that a higher MOI disrupts host Ca^{2+} signaling earlier
628   in infection and sustains this aberrant Ca^{2+} signaling throughout. Mock and irradiated have similar
629   heatmap profiles, suggesting that replication competent virus is required to drive these changes in
630   Ca^{2+} signaling. Data shown as mean $\pm$ SD. **p<0.001, ****p<0.0001.
631
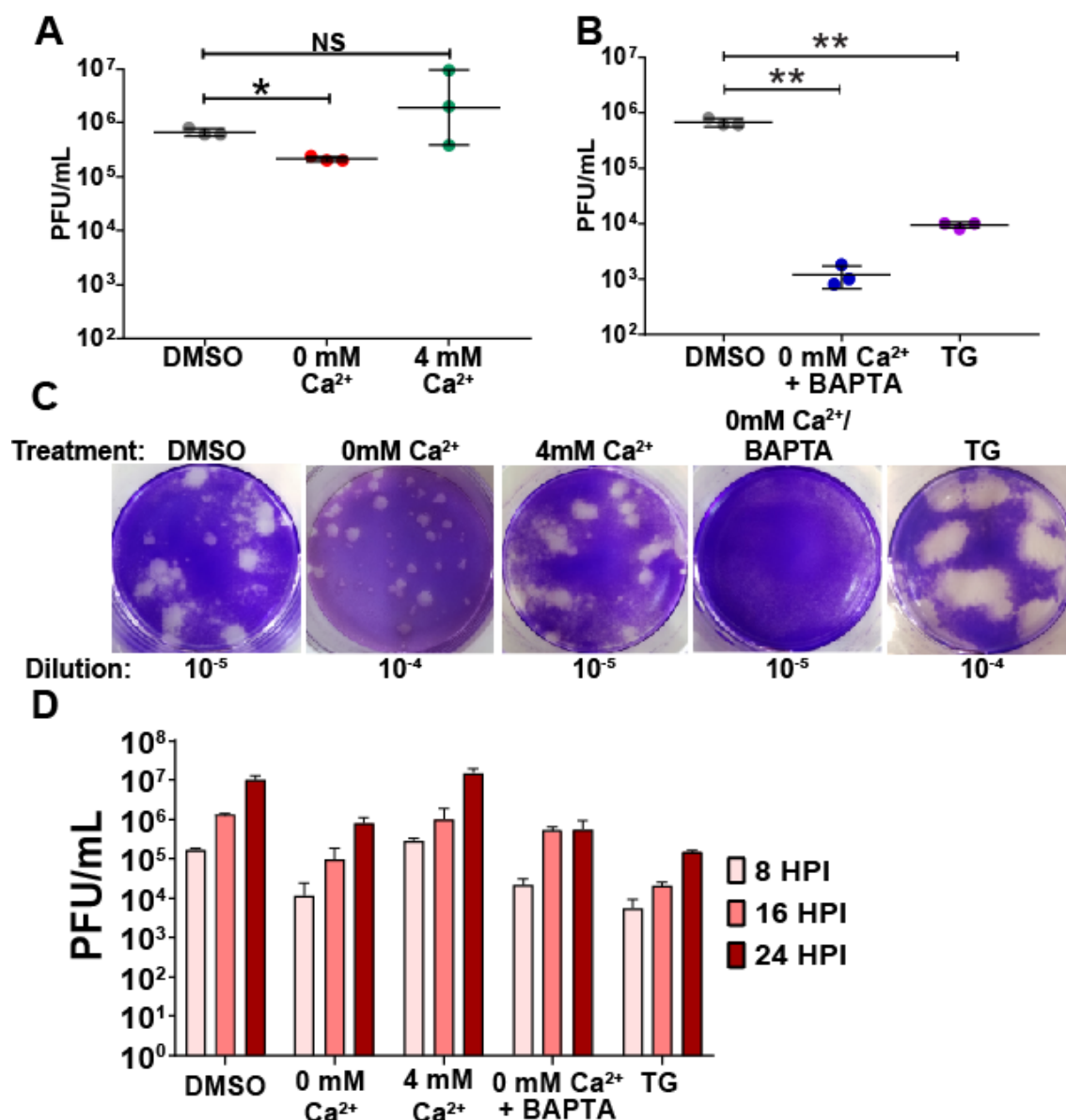
Figure 2: Intracellular calcium is critical for TV replication. A. Buffering out extracellular calcium hinders TV replication, significantly reducing the total plaque forming units (PFU). In contrast, excess extracellular Ca^{2+} (4 mM Ca^{2+}, right) does not impact replication. **B.** Buffering intracellular calcium reduces replication. Depleting ER calcium stores with the SERCA-inhibitor thapsigargin and reducing cytoplasmic Ca^{2+} with BAPTA-AM significantly reduce TV infectious yield (PFU/mL). **C.** Representative images of plaques under normal (2mM) Ca^{2+} conditions (top, DMSO) and reduced Ca^{2+} (0 mM Ca^{2+}/Bapta-AM, TG), conditions (bottom). **D.** Partial one-step growth curve data altering free intracellular (IC) and extracellular (EC) Ca^{2+}. TV replication is stunted in Ca^{2+} free IC and EC conditions (0 mM Ca^{2+}, 0 mM Ca^{2+}/BAPTA-AM). Inhibiting ER Ca^{2+} replenishment with thapsigargin also blunts replication, suggesting that IC Ca^{2+} stores are critical for TV replication. Data shown as mean ± SD. *p<0.01, **p<0.001.

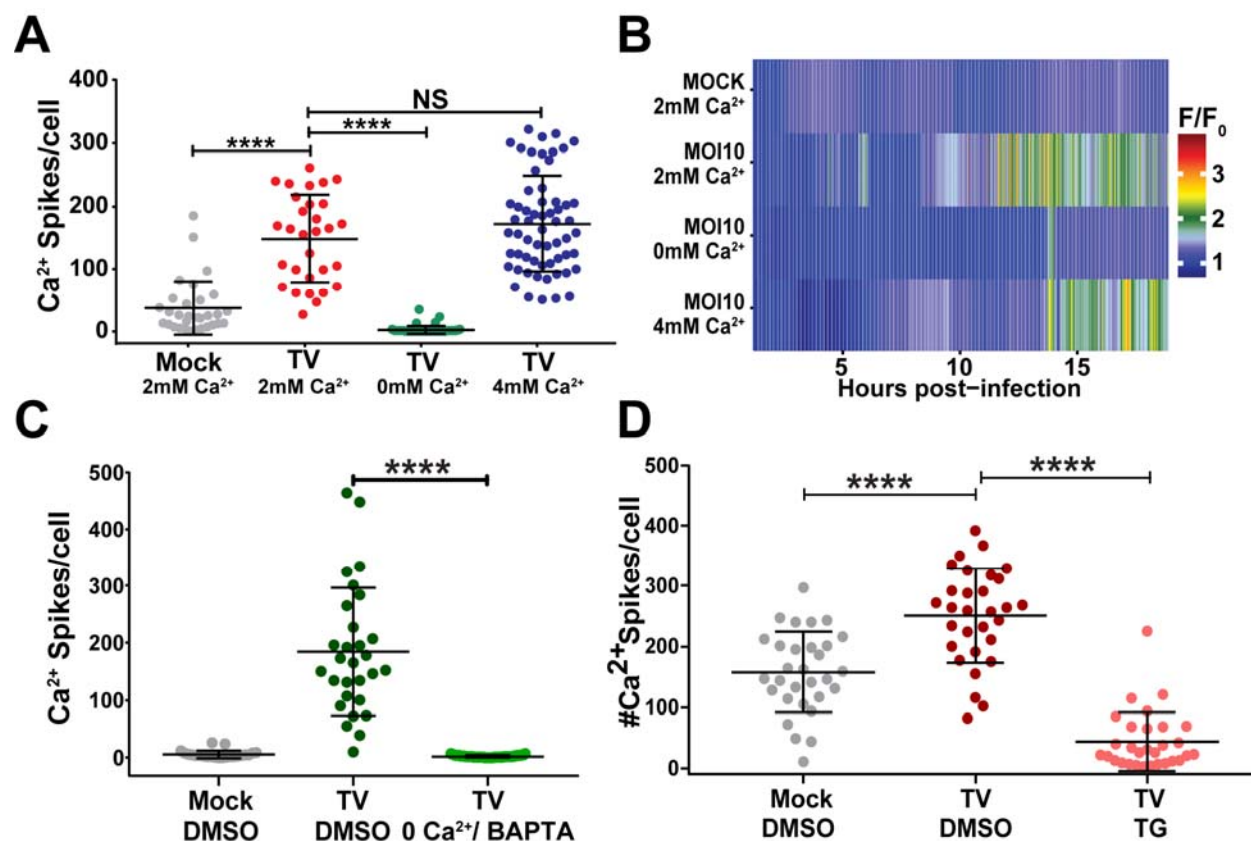**Figure 3: TV-induced Ca^{2+} signaling requires ER Ca^{2+} stores. A**. Ca^{2+}-free media reduces Ca^{2+} signaling in TV-infected cells, suggesting Ca^{2+} signaling is activated during infection. **B.** TV infection in 0 mM Ca^{2+} phenocopies mock Ca^{2+} traces in heatmap data, suggesting that EC Ca^{2+} facilitates TV infection. **C.** Intracellular Ca^{2+} chelator BAPTA-AM abrogated TV-induced Ca^{2+} signaling. BAPTA-AM-treated TV-infected cells (light green) returns Ca^{2+} signaling to uninfected levels (grey). **D.** Depleting ER Ca^{2+} with SERCA blocker thapsigargin (TG) significantly reduces TV-induced Ca^{2+} signaling (pink), suggesting that ER Ca^{2+} stores are a key source of Ca^{2+} leveraged during infection. Data shown as mean ± SD. ****p<0.0001.
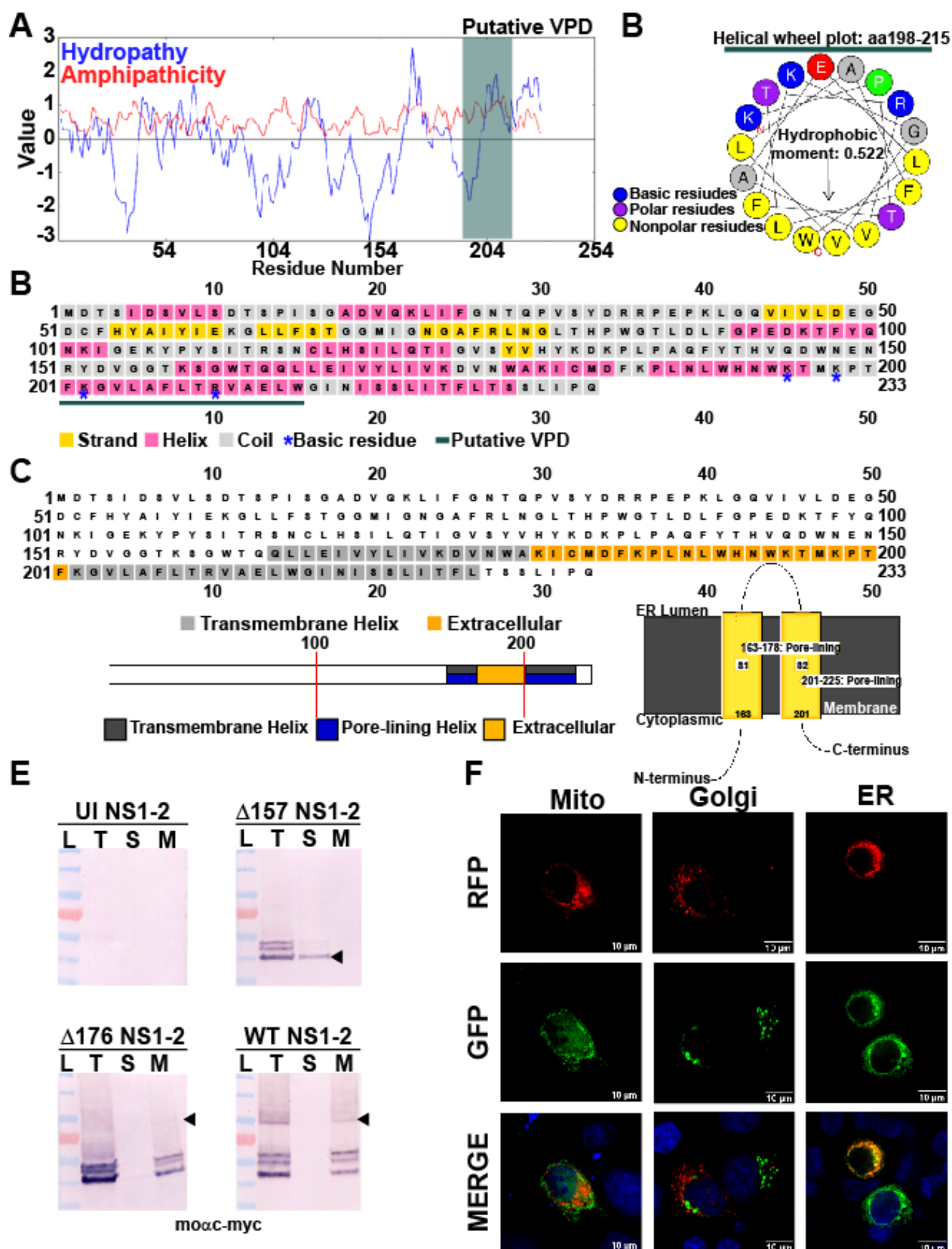
Figure 4: Tulane virus NS1-2 is targeted to the ER membrane. **A.** Predictive modeling of TV NS1-2 reveals that is has essential features of *bona fide* viroporins. Kyte-Doolittle-hydropathy plots predict an amphipathic moment from aa195-212 (dark green bar), consistent with alpha-helical structure required for channel formation. **B.** PSIPred secondary structure algorithms predict the C-terminus of NS1-2 is helical in nature, with the putative viroporin domain (VPD) contained to helices. **C.** PSIPred membrane topology predictions suggest that NS1-2 has two transmembrane helices (grey cubes, top figure). PSIPred algorithms predicting transmembrane helices suggest NS1-2 transmembrane domains are pore-lining (bottom left) and propose a model of membrane insertion and orientation where the putative VPD (aa195-212) comprises the pore-lining helix (bottom right). **D.** Helical wheel plot generated from the NS1-2 amphipathic segment (dark green bar) show clustered basic residues (green asterisks) and a hydrophobic moment of 0.522 from aa198-215, coinciding with the putative VPD **E.** Mammalian expressed full-length RFP-NS1-2 and RFP NS1-2 Δ176 is membrane-associated, but RFP NS1-2 Δ157 is not. Both the total fraction (T) and membrane pellets (M) extracted with 1% SDS contain RFP-NS1-2 and Δ176, but centrifuged supernatant (S) does not, suggesting that RFP-NS1-2 and Δ176 are membrane-associated proteins. In contrast, the supernatant contains RFP-NS1-2 Δ157. Further, immunoblot assays run under non-reducing conditions show that full-length RFP-NS1-2 and Δ176 oligomerize (black arrowheads) **F.** Co-transfection experiments using intracellular markers for predominant intracellular Ca^{2+} stores mitochondria (mito), Golgi, and endoplasmic reticulum (ER) to determine whether TV NS1-2 associated with any intracellular organelle(s). Based on deconvolution microscopy data, RFP-NS1-2 localized to the ER (right), but not with the Golgi (middle). RFP-NS1-2 did not localize to the mitochondria (left) (N≥2).
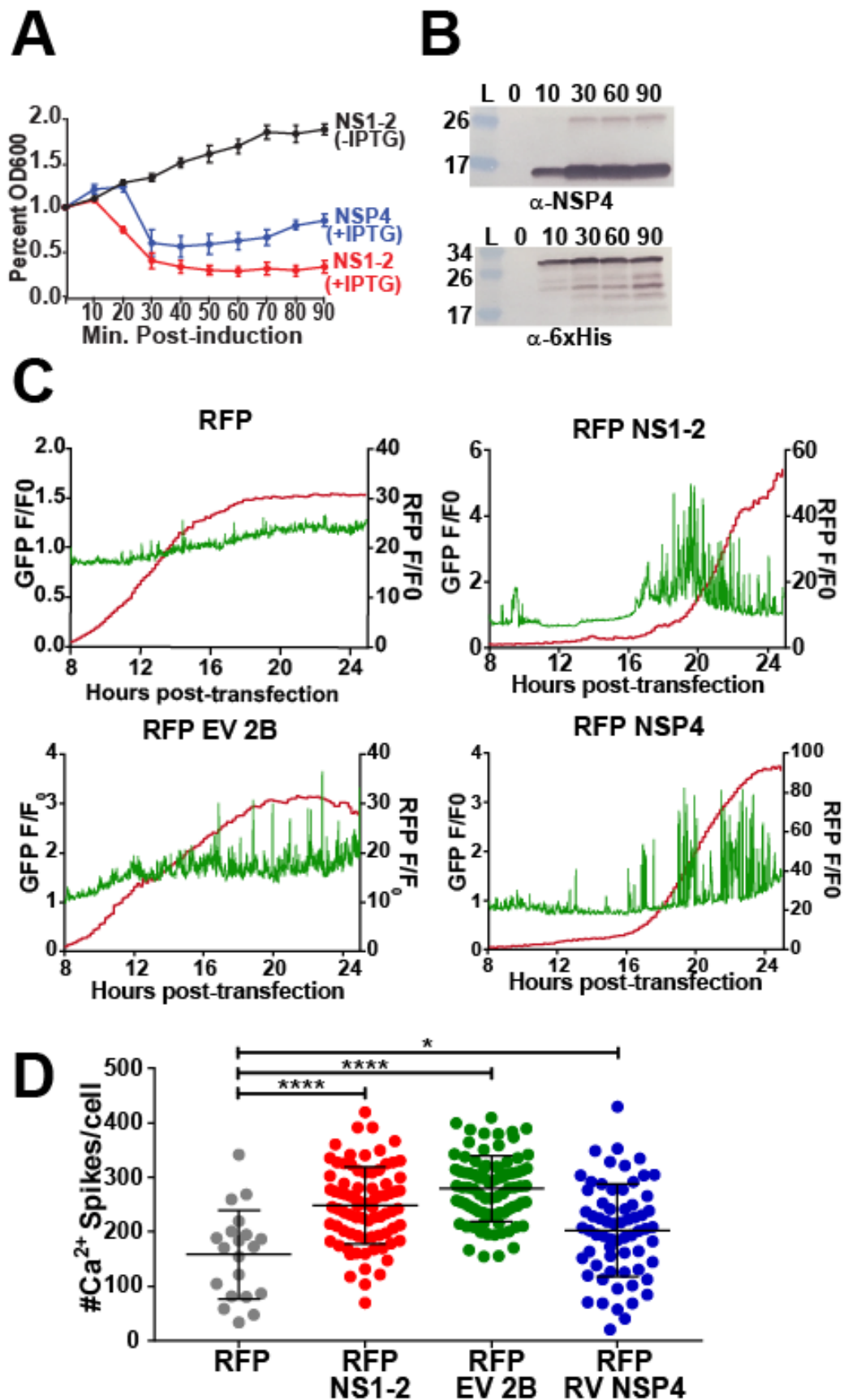
677

678   **Figure 5: V NS1-2 has viroporin activity that disrupts Ca^{2+} signaling in mammalian cells. A.**
679   Inducing TV NS1-2 in the lysis assay strongly reduces optical density similar to rotavirus NSP4,
680   the positive control for viroporin activity. B. Western blot data to verify protein expression
681   during the lysis assay for TV NS1-2 (bottom) and RV NSP4 (top). **C, D.** Mammalian
682   recombinant RFP-NS1-2 increases the number (B) and amplitude (C, top row, right) of Ca^{2+}
683   spikes when transfected into cells similar to RV NSP4 and EV 2B, the viroporin controls for
684   these experiments. Data shown as mean ± SD from ≥8 fields-of-view. *p<0.01, ****p<0.0001.
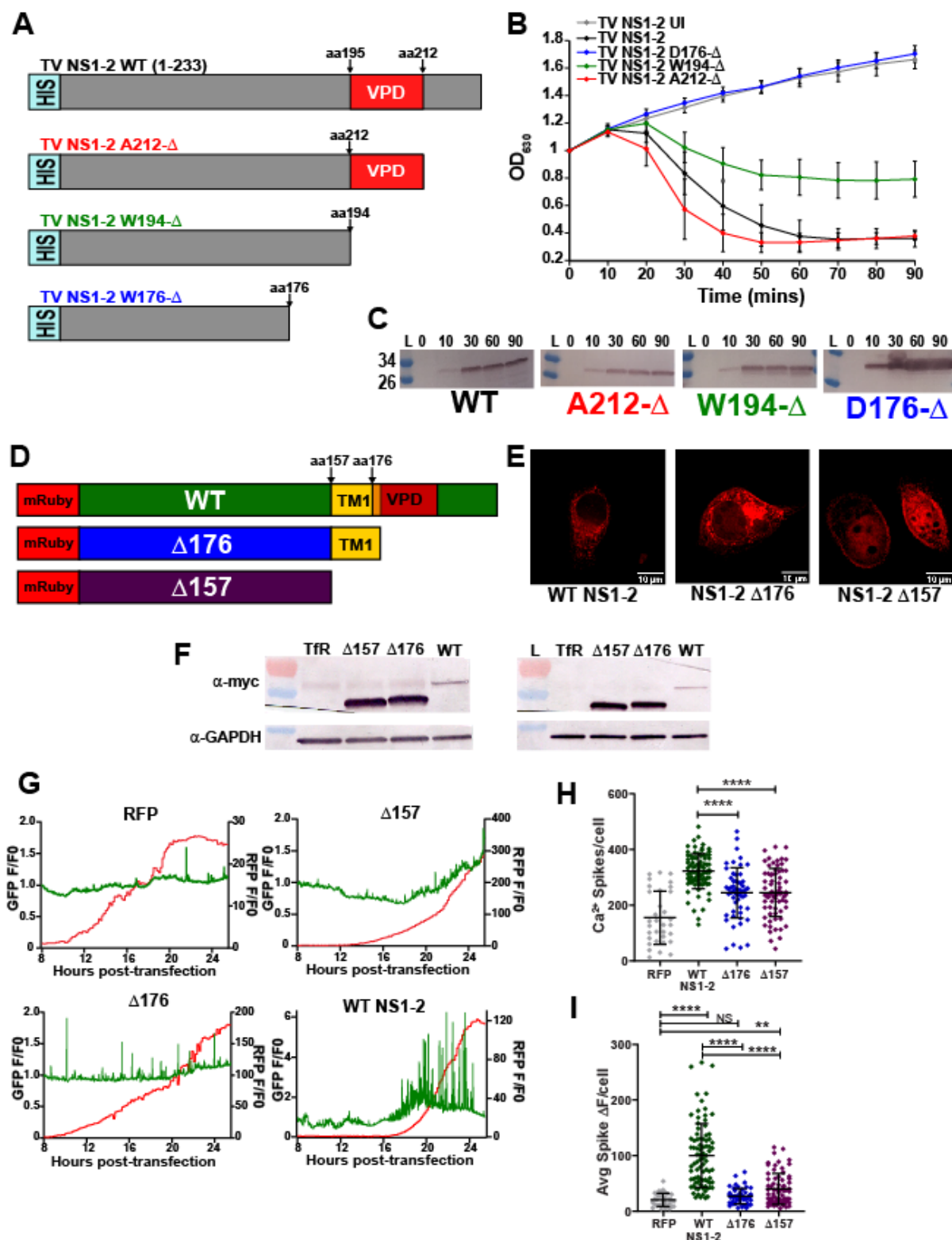685

Figure 6: NS1-2 viroporins mutants do not increase cytoplasmic Ca^{2+} A. Schematic of TV NS1-2 C-terminal truncation mutants to functionally map the viroporin domain. **B.** In the lysis assay, truncating the C-terminal domain to amino acid 212 (red) results in wild-type activity

690   (black), but truncating to W194 (green) impairs activity. Truncating to D176 (blue) abrogates
691   viroporin activity, suggesting the viroporin domain functionally spans from aa177-212. **C.**
692   Western blots verifying protein expression in the lysis assay. **D.** Schematic for the mammalian
693   C-terminal truncation mutant constructs. **E.** IF data for truncation mutants. The Δ157 is
694   cytoplasmic (far right), whereas the Δ176, which retains one transmembrane segment, is
695   membrane localized (middle). **F.** Western blot data confirm the Δ157 and Δ176 mutant
696   constructs. The left blot is run with 20 μL/well to visualize FL NS1-2, whereas the right blot is
697   run with 5 μL/well to resolve the size difference between the Δ157 and 176 NS1-2 mutants. **G.**
698   Both the Δ157 and Δ176 truncation mutants have significantly less Ca^{2+} spikes/cell compared to
699   wild-type full length RFP-NS1-2. **H.** Compared to full length RFP-NS1-2, both the Δ157 and
700   Δ176 truncation mutants have a significant reduced Ca^{2+} spike amplitudes, resulting in a change
701   in cytosolic fluorescence (ΔF) that phenotypically mimics RFP alone. Data shown as mean ± SD
702   from ≥8 fields-of-view. **p<0.001, ****p<0.0001.
703

References

1. Wobus CE, Cunha JB, Elftman M, Kolawole AO. 2016. Animal Models of Norovirus Infection, p. 397–415. *In* Svensson, L, Desselberger, U, Greenberg, HB, Estes, MK (eds.), Viral Gastroenteritis: Molecular Epidemiology and Pathogenesis. Academic Press, Cambridge, MA.

2. Kniel KE. 2014. The makings of a good human norovirus surrogate. Curr Opin Virol 4:85–90.

3. Desselberger U. 2019. Caliciviridae Other Than Noroviruses. Viruses 11:286.

4. Karst SM, Wobus CE, Goodfellow IG, Green KY, Virgin HW. 2014. Advances in norovirus biology. Cell Host Microbe 15:668–680.

5. Li J, Predmore A, Divers E, Lou F. 2012. New Interventions Against Human Norovirus: Progress, Opportunities, and Challenges. Annu Rev Food Sci Technol 3:331–352.

6. Pendu J Le, Rydell GE, Nasir W, Larson G. 2016. Chapter 3.3 - Human Norovirus Receptors, p. 379–396. *In* Svensson, L, Desselberger, U, Greenberg, HB, Estes, MK (eds.), Viral Gastroenteritis. Academic Press, Cambridge, MA.

7. Ettayebi K, Crawford SE, Murakami K, Broughman JR, Karandikar U, Tenge VR, Neill FH, Blutt SE, Zeng X-L, Qu L, Kou B, Opekun AR, Burrin D, Graham DY, Ramani S, Atmar RL, Estes MK. 2016. Replication of human noroviruses in stem cell-derived human enteroids. Science (80-) 353:1387–1393.

8. Bartnicki E, Cunha JB, Kolawole AO, Wobus CE. 2017. Recent advances in understanding noroviruses. F1000Research 6:79.

9. Richardson C, Bargatze RF, Goodwin R, Mendelman PM. 2013. Norovirus virus-like particle vaccines for the prevention of acute gastroenteritis. Expert Rev Vaccines 12:155–167.

10. Ramani S, Atmar RL, Estes MK. 2014. Epidemiology of human noroviruses and updates on vaccine development. Curr Opin Gastroenterol 30:25–33.

11. Farkas T, Sestak K, Wei C, Jiang X. 2008. Characterization of a Rhesus Monkey Calicivirus Representing a New Genus of Caliciviridae. J Virol 82:5408–5416.

12. Wei C, Farkas T, Sestak K, Jiang X. 2008. Recovery of Infectious Virus by Transfection of In Vitro-Generated RNA from Tulane Calicivirus cDNA. J Virol 82:11429–11436.

13. Smits SL, Rahman M, Schapendonk CME, van Leeuwen M, Faruque ASG, Haagmans BL, Endtz HP, Osterhaus ADME. 2012. Calicivirus from novel recovirus genogroup in human diarrhea, Bangladesh. Emerg Infect Dis 18:1192–1195.

14. Goodfellow IG, Taube S. 2016. Calicivirus Replication and Reverse Genetics, p. 355–378. *In* Svensson, L, Desselberger, U, Greenberg, HB, Estes, MK (eds.), Viral Gastroenteritis: Molecular Epidemiology and Pathogenesis. Academic Press, Cambridge, MA.

15. Farkas T. 2015. Rhesus enteric calicivirus surrogate model for human norovirus gastroenteritis. J Gen Virol 96:1504–1514.

16. Green KY. 2013. The Noroviruses, p. 949–979. *In* Knipe, D, Howley, P (eds.), Field's Virology, 6th ed. Wolter Kluwer Health/Lippincott Williams & Wilkins, Philadelphia, PA.

17. Bailey D, Kaiser WJ, Hollinshead M, Moffat K, Chaudhry Y, Wileman T, Sosnovtsev S V., Goodfellow IG. 2010. Feline calicivirus p32, p39 and p30 proteins localize to the endoplasmic reticulum to initiate replication complex formation. J Gen Virol 91:739–749.

18. Hyde JL, Mackenzie JM. 2010. Subcellular localization of the MNV-1 ORF1 proteins and their potential roles in the formation of the MNV-1 replication complex. Virology 406:138–148.

19. Lee S, Liu H, Wilen CB, Sychev ZE, Desai C, Hykes BL, Orchard RC, McCune BT, Kim K-W, Nice TJ, Handley SA, Baldridge MT, Amarasinghe GK, Virgin HW. 2019. A Secreted Viral Nonstructural Protein Determines Intestinal Norovirus Pathogenesis. Cell Host Microbe 1–13.

20. Urakova N, Frese M, Hall RN, Liu J, Matthaei M, Strive T. 2015. Expression and partial characterisation of rabbit haemorrhagic disease virus non-structural proteins. Virology 484:69–79.

21. Doerflinger SY, Cortese M, Romero-Brey I, Menne Z, Tubiana T, Schenk C, White PA, Bartenschlager R, Bressanelli S, Hansman GS, Lohmann V. 2017. Membrane alterations induced by nonstructural proteins of human norovirusPLoS Pathogens.

22. Lee S, Wilen CB, Orvedahl A, McCune BT, Kim KW, Orchard RC, Peterson ST, Nice TJ, Baldridge MT, Virgin HW. 2017. Norovirus Cell Tropism Is Determined by Combinatorial Action of a Viral Non-structural Protein and Host Cytokine. Cell Host Microbe 22:449-459.e4.

23. Fernandez-Vega V, Sosnovtsev S V, Belliot G, King AD, Mitra T, Gorbalenya A, Green KY. 2004. Norwalk virus N-terminal nonstructural protein is associated with disassembly of the Golgi complex in transfected cells. J Virol 78:4827–37.

24. Ettayebi K, Hardy ME. 2003. Norwalk virus nonstructural protein p48 forms a complex with the SNARE regulator VAP-A and prevents cell surface expression of vesicular stomatitis virus G protein. J Virol 77:11790–7.

25. Jing J, He L, Sun A, Quintana A, Ding Y, Ma G, Tan P, Liang X, Zheng X, Chen L, Shi X, Zhang SL, Zhong L, Huang Y, Dong M-Q, Walker CL, Hogan PG, Wang Y, Zhou Y. 2015. Proteomic mapping of ER–PM junctions identifies STIMATE as a regulator of Ca^{2+} influx SUPPLEMENTARY. Nat Cell Biol 17:1339–1347.

26. Raffaello A, Mammucari C, Gherardi G, Rizzuto R. 2016. Calcium at the Center of Cell Signaling: Interplay between Endoplasmic Reticulum, Mitochondria, and Lysosomes. Trends Biochem Sci 41:1035–1049.

27. Cui C, Merritt R, Fu L, Pan Z. 2017. Targeting calcium signaling in cancer therapy. Acta Pharm Sin B 7:3–17.

28. Carafoli E, Krebs J. 2016. Why calcium? How calcium became the best communicator. J Biol Chem 291:20849–20857.

29. Gudermann T, Mederos y Schnitzler M, Dietrich A. 2004. Receptor-Operated Cation Entry--More Than Esoteric Terminology? Sci Signal 2004:pe35–pe35.

30. Zhou Y, Frey TK, Yang JJ. 2009. Viral Calciomics: Interplays between Ca2+ and virus. Cell Calcium 46:1–17.

31. Bagur R, Hajnóczky G. 2017. Intracellular Ca2+ Sensing: Its Role in Calcium Homeostasis and Signaling. Mol Cell 66:780–788.

32. Dickson EJ, Jensen JB, Hille B. 2016. Regulation of calcium and phosphoinositides at endoplasmic reticulum–membrane junctions. Biochem Soc Trans 44:467–476.

33. Nieto-Torres JL, Verdiá-Báguena C, Castaño-Rodriguez C, Aguilella VM, Enjuanes L. 2015. Relevance of viroporin ion channel activity on viral replication and pathogenesis. Viruses 7:3552–3573.

34. Nieva JL, Madan V, Carrasco L. 2012. Viroporins: Structure and biological functions. Nat Rev Microbiol 10:563–574.

35. Sze CW, Tan YJ. 2015. Viral membrane channels: Role and function in the virus life cycle. Viruses 7:3261–3284.

36. Hyser JM, Collinson-Pautz MR, Utama B, Estes MK. 2010. Rotavirus disrupts calcium homeostasis by NSP4 viroporin activity. MBio 1:1–12.

37. Van Kuppeveld FJM, De Jong AS, Melchers WJG, Willems PHGM. 2005. Enterovirus protein 2B po(u)res out the calcium: A viral strategy to survive? Trends Microbiol 13:41–44.

38. Wang K, Xie S, Sun B. 2011. Viral proteins function as ion channels. Biochim Biophys Acta - Biomembr 1808:510–515.

39. Hyser JM, Estes MK. 2015. Pathophysiological Consequences of Calcium-Conducting Viroporins. Annu Rev Virol 2:473–496.

40. Hyser JM, Estes MK. 2009. Rotavirus Vaccines and Pathogenesis: 2008. Curr Opin Gastroenterol 25:36–43.

41. Pham T, Perry JL, Dosey TL, Delcour AH, Hyser JM. 2017. The Rotavirus NSP4 Viroporin Domain is a Calcium-conducting Ion Channel. Sci Rep 7:1–11.

42. van Kuppeveld FJ, Galama JM, Zoll J, Melchers WJ. 1995. Genetic analysis of a hydrophobic domain of coxsackie B3 virus protein 2B: a moderate degree of hydrophobicity is required for a cis-acting function in viral RNA synthesis. J Virol 69:7782–90.

43. de Jong AS, de Mattia F, Van Dommelen MM, Lanke K, Melchers WJG, Willems PHGM, van Kuppeveld FJM. 2008. Functional Analysis of Picornavirus 2B Proteins: Effects on Calcium Homeostasis and Intracellular Protein Trafficking. J Virol 82:3782–3790.

44. Martinez-Gil L, Bano-Polo M, Redondo N, Sanchez-Martinez S, Nieva JL, Carrasco L, Mingarro I. 2011. Membrane Integration of Poliovirus 2B Viroporin. J Virol 85:11315–

820   11324.

821   45.   Koonin E V, Dolja V V. 1993. Evolution and taxonomy of positive-strand viruses:
822   Implications and analysis of amino acid sequences. Crit Rev Biochem Mol Biol 28:375–
823   430.

824   46.   Zell R. 2017. Picornaviridae—the ever-growing virus family. Arch Virol 163:1–19.

825   47.   Chang-Graham AL, Perry JL, Strtak AC, Ramachandran NK, Criglar JM, Philip AA,
826   Patton JT, Estes MK, Hyser JM. 2019. Rotavirus Calcium Dysregulation Manifests as
827   Dynamic Calcium Signaling in the Cytoplasm and Endoplasmic Reticulum. BioRxiv 1–
828   19.

829   48.   Hadley A, Henry L. 2019. Package "tidyr": Easily Tidy Data with "spread()" and
830   "gather()" Functions.

831   49.   Wickham H. 2009. ggplot2: Elegant Graphics for Data Analysis, p. 1–16. *In* Valero-Mora,
832   PM (ed.), UseR! Springer-Verlag, New York.

833   50.   Saier MH. 2005. TCDB: the Transporter Classification Database for membrane transport
834   protein analyses and information. Nucleic Acids Res 34:D181–D186.

835   51.   Buchan DWA, Jones DT. 2019. The PSIPRED Protein Analysis Workbench: 20 years on.
836   Nucleic Acids Res 1–6.

837   52.   Gautier R, Douguet D, Antonny B, Drin G. 2008. HELIQUEST: A web server to screen
838   sequences with specific α-helical properties. Bioinformatics 24:2101–2102.

839   53.   Hyser JM, Utama B, Crawford SE, Broughman JR, Estes MK. 2013. Activation of the
840   Endoplasmic Reticulum Calcium Sensor STIM1 and Store-Operated Calcium Entry by
841   Rotavirus Requires NSP4 Viroporin Activity 87:13579–13588.

842   54.   Nan X, Hyndman L, Agbi N, Porteous DJ, Boyd AC. 2004. Potent stimulation of gene
843   expression by histone deacetylase inhibitors on transiently transfected DNA. Biochem
844   Biophys Res Commun 324:348–354.

845   55.   Lu HK, Gray LR, Wightman F, Ellenberg P, Khoury G, Cheng WJ, Mota TM, Wesselingh
846   S, Gorry PR, Cameron PU, Churchill MJ, Lewin SR. 2014. Ex vivo response to histone
847   deacetylase (HDAC) inhibitors of the HIV long terminal repeat (LTR) derived from HIV-
848   infected patients on antiretroviral therapy. PLoS One 9.

849   56.   Paszkiet BJ, Zhang J, Matukonis M, Kaleko M, Luo T. 2016. Histone Deacetylation
850   Inhibitors Enhance Lentiviral Vector Production and Infectivity. Mol Ther 5:S308.

851   57.   Schneider CA, Rasband WS, Eliceiri KW. 2012. NIH Image to ImageJ: 25 years of image
852   analysis. Nat Methods 9:671–5.

853   58.   Chen T-W, Wardill TJ, Sun Y, Pulver SR, Renninger SL, Baohan A, Schreiter ER, Kerr
854   RA, Orger MB, Jayaraman V, Looger LL, Svoboda K, Kim DS. 2013. Ultrasensitive
855   fluorescent proteins for imaging neuronal activity. Nature 499:295–300.

856   59.   Billman GE. 1993. Intracellular calcium chelator, BAPTA-AM, prevents cocaine-induced
857   ventricular fibrillation. Am J Physiol Circ Physiol H1529–H1535.

858 60. Horvath B, Szentandrassy N, Veress R, Baranyai D, Kistamas K, Almassy J, Toth A,
859   Magyar J, Banyasz T, Nanasi PP. 2018. Effect of the intracellular calcium concentration
860   chelator BAPTA acetoxy-methylester on action potential duration in canine ventricular
861   myocytes. J Physiol Pharmacol 69:99–107.

862 61. Gonzalez ME, Carrasco L. 2003. Viroporins. FEBS Lett 552:28–34.

863 62. Neil JD. 1990. Nucleotide sequence of a region of the feline calicivirus genome which
864   encodes picornavirus-like RNA-dependent RNA polymerase , cysteine protease and 2C
865   polypeptides. Virus Res 17:145–160.

866 63. Kuyumcu-Martinez M, Belliot G, Sosnovtsev S V., Chang K-O, Green KY, Lloyd RE.
867   2004. Calicivirus 3C-Like Proteinase Inhibits Cellular Translation by Cleavage of
868   Poly(A)-Binding Protein. J Virol 78:8172–8182.

869 64. Venkataraman S, Prasad BVLS, Selvarajan R. 2018. RNA dependent RNA polymerases:
870   Insights from structure, function and evolution. Viruses 10:1–23.

871 65. Lama J, Carrasco L. 1992. Expression of poliovirus nonstructural proteins in Escherichia
872   coli cells. J Biol Chem 267:15932–15937.

873 66. Guinea R, Carrasco L. 1994. Influenza virus M2 protein modifies membrane permeability
874   in E. coli cells. FEBS Lett 343:242–246.

875 67. Crawford SE, Estes MK. 2013. Viroporin-mediated calcium-activated autophagy 797–
876   798.

877 68. Furlong K, Hwang S. 2019. Autophagy and Noroviruses. Viruses 11:244.

878 69. Krebs J, Agellon LB, Michalak M. 2015. Ca2+ homeostasis and endoplasmic reticulum
879   (ER) stress: An integrated view of calcium signaling. Biochem Biophys Res Commun
880   460:114–121.

881 70. van Kuppeveld FJ, Galama JM, Zoll J, van den Hurk PJ, Melchers WJ. 1996. Coxsackie
882   B3 virus protein 2B contains cationic amphipathic helix that is required for viral RNA
883   replication. J Virol 70:3876–3886.

884 71. Lock JT, Alzayady KJ, Yule DI, Parker I. 2018. All three IP 3 receptor isoforms generate
885   Ca 2+ puffs that display similar characteristics . Sci Signal 11:eaau0344.

886 72. Taylor CW, Tovey SC. 2010. IP3 Receptors: Toward Understanding Their Activation.
887   Cold Spring Harb Perspect Biol 1–23.

888 73. Jin X, Shah S, Du X, Zhang H, Gamper N. 2016. Activation of Ca2+-activated Cl-
889   channel ANO1 by localized Ca2+ signals. J Physiol 594:19–30.

890 74. Concepcion AR, Vaeth M, Wagner LE, Eckstein M, Hecht L, Jun Y, Crottes D, Seidl M,
891   Shin HP, Weidinger C, Cameron S, Turvey SE, Issekutz T, Meyts I, Lacruz RS, Cuk M,
892   Yule DI, Feske S. 2016. Store-operated Ca2+ entry regulates Ca2+-activated chloride
893   channels and eccrine sweat gland function. J Clin Invest 126:4303–4318.

894